Pure optical photoacoustic microscopy

Zhixing Xie,[1,3] Sung-Liang Chen,[2,3] Tao Ling,[2,3] L. Jay Guo,[2,4] Paul L. Carson,[1,5] Xueding Wang[1,*]

[1]*Department of Radiology, University of Michigan, Ann Arbor, Michigan 48109, USA*
[2]*Department of Electrical Engineering and Computer Science, University of Michigan, Ann Arbor, Michigan 48109, USA*
[3]*These authors contributed equally to this work*
[4]*guo@umich.edu*
[5]*pcarson@umich.edu*
[*]*xdwang@umich.edu*

Abstract: The concept of pure optical photoacoustic microscopy(POPAM) was proposed based on optical rastering of a focused excitation beam and optically sensing the photoacoustic signal using a microring resonator fabricated by a nanoimprinting technique. After the refinements of the microring's working wavelength and in the resonator structure and mold fabrication, an ultrahigh Q factor of 3.0×10^5 was achieved which provided high sensitivity with a noise equivalent detectable pressure(NEDP) value of 29Pa. This NEDP is much lower than the hundreds of Pascals achieved with existing optical resonant structures such as etalons, fiber gratings and dielectric multilayer interference filters available for acoustic measurement. The featured high sensitivity allowed the microring resonator to detect the weak photoacoustic signals from micro- or submicroscale objects. The inherent superbroad bandwidth of the optical microring resonator combined with an optically focused scanning beam provided POPAM with high resolution in the axial as well as both lateral directions while the axial resolution of conventional photoacoustic microscopy (PAM) suffers from the limited bandwidth of PZT detectors. Furthermore, the broadband microring resonator showed similar sensitivity to that of our most sensitive PZT detector. The current POPAM system provides a lateral resolution of 5 μm and an axial resolution of 8 μm, comparable to that achieved by optical microscopy while presenting the unique contrast of optical absorption and functional information complementing other optical modalities. The 3D structure of microvasculature, including capillary networks, and even individual red blood cells have been discerned successfully in the proof-of-concept experiments on mouse bladders ex vivo and mouse ears in vivo. The potential of approximately GHz bandwidth of the microring resonator also might allow much higher resolution than shown here in microscopy of optical absorption and acoustic propagation properties at depths in unfrozen tissue specimens or thicker tissue sections, which is not now imageable with current optical or acoustic microscopes of comparable resolution.

OCIS codes: (230.5750) Resonators; (110.5120) Photoacoustic imaging; (110.0180) Microscopy.

References and links

1. M. Fernandez-Suarez, and A. Y. Ting, "Fluorescent probes for super-resolution imaging in living cells," Nat. Rev. Mol. Cell Biol. **9**(12), 929–943 (2008).
2. E. Betzig, G. H. Patterson, R. Sougrat, O. W. Lindwasser, S. Olenych, J. S. Bonifacino, M. W. Davidson, J. Lippincott-Schwartz, and H. F. Hess, "Imaging Intracellular Fluorescent Proteins at Nanometer Resolution," Science **313**(5793), 1642–1645 (2006).
3. M. G. L. Gustafsson, "Nonlinear structured-illumination microscopy: wide-field fluorescence imaging with theoretically unlimited resolution," Proc. Natl. Acad. Sci. U.S.A. **102**(37), 13081–13086 (2005).
4. X. Zhuang, "Nano-imaging with Storm," Nat. Photonics **3**(7), 365–367 (2009).

#142134 - $15.00 USD Received 9 Feb 2011; revised 4 Apr 2011; accepted 10 Apr 2011; published 25 Apr 2011

5. H. F. Zhang, K. Maslov, G. Stoica, and L. V. Wang, "Functional photoacoustic microscopy for high-resolution and noninvasive in vivo imaging," Nat. Biotechnol. **24**(7), 848–851 (2006).
6. K. Maslov, H. F. Zhang, S. Hu, and L. V. Wang, "Optical-resolution photoacoustic microscopy for in vivo imaging of single capillaries," Opt. Lett. **33**(9), 929–931 (2008).
7. Z. Xie, S. Jiao, H. F. Zhang, and C. A. Puliafito, "Laser-scanning optical-resolution photoacoustic microscopy," Opt. Lett. **34**(12), 1771–1773 (2009).
8. X. Wang, Y. Pang, G. Ku, X. Xie, G. Stoica, and L. V. Wang, "Noninvasive laser-induced photoacoustic tomography for structural and functional in vivo imaging of the brain," Nat. Biotechnol. **25**(7), 114–116 (2003).
9. L. V. Wang, "Tutorial on photoacoustic microscopy and computed tomography," IEEE J. Sel. Top. Quantum Electron. **14**(1), 171–179 (2008).
10. S. Ashkenazi, C.-Y. Chao, L. J. Guo, M. O'Donnell; "Ultrasound detection using polymer microring optical resonator," Appl. Phys. Lett. **85**(22), 5418–5420 (2004).
11. E. Zhang, J. Laufer, and P. Beard, "Backward-mode multiwavelength photoacoustic scanner using a planar Fabry-Perot polymer film ultrasound sensor for high-resolution three-dimensional imaging of biological tissues," Appl. Opt. **47**(4), 561–577 (2008).
12. S. W. Huang, S. L. Chen, T. Ling, A. Maxwell, M. O'Donnell, L. J. Guo, and S. Ashkenazi, "Low-noise wideband ultrasound detection using polymer microring resonators," Appl. Phys. Lett. **92**(19), 193509 (2008).
13. H. Won Baac, J. G. Ok, H. J. Park, T. Ling, S. L. Chen, A. J. Hart, and L. J. Guo, "Carbon nanotube composite optoacoustic transmitters for strong and high frequency ultrasound generation," Appl. Phys. Lett. **97**(23), 234104 (2010).
14. C. Y. Chao, and L. J. Guo, "Polymer microring resonators fabricated by nanoimprint technique," J. Vac. Sci. Technol. B **20**(6), 2862–2866 (2002).
15. T. Ling, S. L. Chen, and L. J. Guo, "Fabrication and characterization of high Q polymer microring resonator and its application as a sensitive ultrasonic detector," Opt. Express **19**(2), 861–869 (2011).
16. P. C. Beard, F. Perennes, and T. N. Mills, "Transduction mechanisms of the Fabry-Perot polymer film sensing concept for wideband ultrasound detection," IEEE Trans. Ultrason. Ferroelectr. Freq. Control **46**(6), 1575–1582 (1999).
17. D. K. Armani, T. J. Kippenberg, S. M. Spillane, and K. J. Vahala, "Ultra-high-Q toroid microcavity on a chip," Nature **421**(6926), 925–928 (2003).

1. Introduction

For imaging by optical scattering and fluorescence, leading edge technologies for modern optical microscopy have entered the realm of super resolution [1–4], breaking the diffraction limit. For three-dimensional functional imaging of optical absorbance, the current photoacoustic microscopy (PAM) technique [5] has quite poor axial resolution, tens to hundreds of microns often seen in ultrasound imaging. This is despite the fact that PAM has recently achieved lateral resolution on the order of a micron, comparable to that of optical microscopy [6, 7]. In PAM, short-pulsed laser light is used to illuminate a tissue sample and generate broadband photoacoustic signals due to differential thermoelastic expansion. The signals can be measured at one or many locations by one or many small or focused ultrasound detectors. Precise summation of these signals can produce an image of the sample, representing the spatial distributions of optical absorbers or functional properties. Such images are highly sensitive to molecular conformation of biological tissues and can aid in describing tissue metabolic and hemodynamic changes [8, 9]. As a novel hybrid imaging modality, PAM provides the unique contrast of optical absorption and scalable penetration exceeding the mean free path of near infrared (NIR) light (on the order of 1 mm). These properties offer the prospect of noninvasive diagnosis and therapeutic monitoring of tissues complementing the range of the depth and resolution of coherence optical tomography and other optical techniques.

With the hope that PAM can achieve high resolution in both lateral and axial dimensions, the concept of pure optical photoacoustic microscopy (POPAM) is proposed. In POPAM, a thin film optical resonator is used to replace the piezoelectric acoustic receivers. The inherent broad band response of the optical thin film structure to acoustic waves, combined with rastering of a focused optical excitation beam can produce both axial resolution and lateral resolution comparable to that achieved in optical microscopy. The high resolution, immunity to electromagnetic interference and good biocompatibility of POPAM open an opportunity to molecular imaging with less invasive and more convenient methodology.

POPAM is not only a novel receiver for PAM, but it also paves the way for exploration of imaging the contrast of optical absorbance on the micron and submicron scale. Even super resolution, breaking the limitations of diffraction, is possible in the future. Though resonant

#142134 - $15.00 USD Received 9 Feb 2011; revised 4 Apr 2011; accepted 10 Apr 2011; published 25 Apr 2011

optical structures such as etalons, fiber gratings and dielectric multilayer interference filters have been studied as ultrasound sensing elements for photoacoustic measurement or tomography [10, 11], in microscopy the photoacoustic signals from micro- or submicro-scale objects, such as capillaries and individual red blood cells, have higher frequency components and are much weaker than those from the larger vasculature observed in tomography. Achieving some of the potential of POPAM has been a challenge.

In this paper, our proof-of-concept studies aim to construct a POPAM prototype and demonstrate its superior resolution capabilities. The preliminary results for imaging mouse bladder ex vivo and mouse ear in vivo suggest excellent performance of POPAM over conventional PAM.

2. Methods and results

Figure 1(a) presents the schematic of a POPAM setup based on the highly sensitive broad bandwidth microring resonator. The resonator has ring-shaped form coupled with a straight waveguide serving as optical input and output. Such microring detectors have been shown to have an almost flat band response up to ~100 MHz [12, 13]. The microring resonator fabricated on a silicon chip was covered by a Mylar protective layer to screen out the exciting laser beam from a Nd:YAG laser (Spot-10-200-532, Elforlight Ltd, UK) . The Nd:YAG laser working at 532nm wavelength has a pulse duration of 2ns and a repetition rate (PRR) of 1KHz. The laser light was spatially filtered by an iris and then expanded to a parallel beam which was rastered over the tissue object by 2D Galvanometers. The intensity and the stability of the laser beam was monitored and calibrated by a photodiode (DET10A, Thorlabs, NJ). An achromatic lens with a focal length of 50 mm was used as the objective lens. On the Mylar protective layer, one coupling pad layer was used to optimize the coupling of the photoacoustic signal from the sample into the microring resonator detector. A tunable laser (TLB-6312, New Focus, CA) provided the light source for the microring resonator at a wavelength tuned to the maximal slope of the resonance peak of the microring's transmission spectrum. A low noise photodiode (1801-FC, New Focus, CA) was used to record the change of the intensity of the light through the microring resonator which reflects the waveform of the photoacoustic signal. The photodetector has a DC output gain of 1 V/mA and AC output gain of 40 V/mA with nominal −6dB electrical bandwidth of 25kHz-125MHz. By sweeping the tunable laser wavelength and using the DC output, the microring's transmission spectrum can be measured. Throughout the experiment, a commercial calibrated Onda transducer (HNC-1500, Onda, CA) with −10dB bandwidth of 300kHz-20MHz was utilized to realize conventional PAM as a control to evaluate the performance of the POPAM. The PAM with Onda transducer shared the same optical focusing and scanning components with POPAM. The Onda transducer operated on a reflection mode at a same distance from the target as the microring resonator working on a transmission mode.

#142134 - $15.00 USD Received 9 Feb 2011; revised 4 Apr 2011; accepted 10 Apr 2011; published 25 Apr 2011

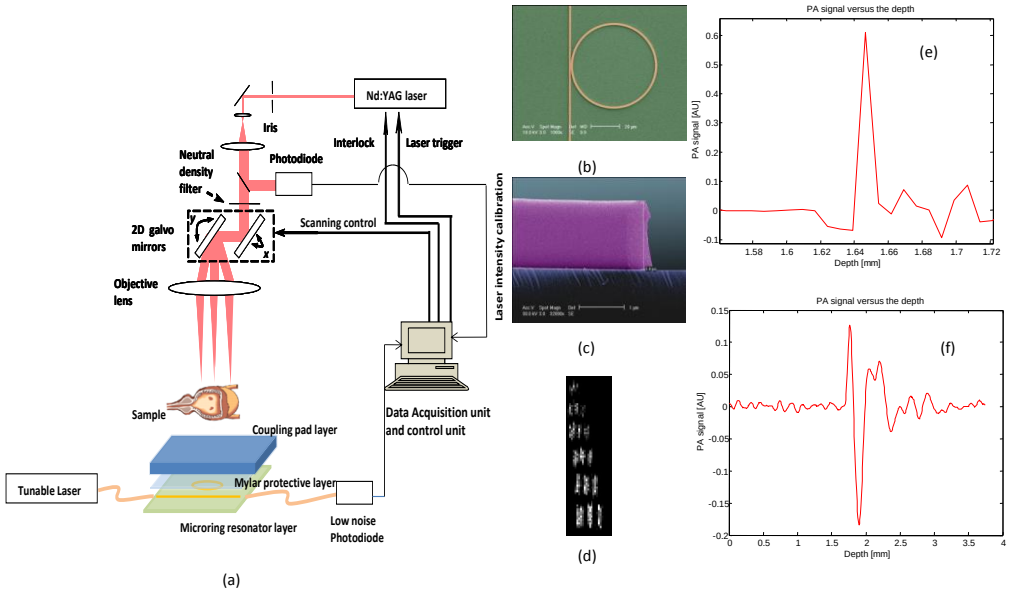

Fig. 1. (a) schematic of a preliminary POPAM system based on a microring resonator. Figure (b) Scanning electron micrograph(SEM) of a polystyrene microring resonator with R=30 μm coupled with a straight waveguide. (c) SEM of the smooth sidewall of a cleaved polymer microring resonator. The height of the waveguide is around 1.4 μm. (d) maximum amplitude projection (MAP) image of the USAF resolution template group 7. (e) A-line signal along the Z axis of the image of the USAF resolution template with POPAM. (f) A-line signal along the Z axis of the image of the USAF resolution template based on conventional PAM with Onda transducer.

In a microring resonator, when the round-trip phase change of optical wave propagating in the ring waveguide is equal to $2m\pi$ (m an integer), the resonance condition is satisfied and the total field of optical wave returning to the coupler is anti-phase with the optical wave propagating through the coupler region in the straight waveguide, resulting in resonance dip in the transmission spectrum. In the presence of ultrasound, acoustic waves deform the polymer waveguide and change the refractive index of the waveguide via elasto-optic effect, and consequently modulate the effective refraction index of the guided mode, leading to a shift of resonance wavelength. At a fixed wavelength corresponding to a high slope in the transmission spectrum, the resonance modulation by the acoustic wave is transformed into intensity modulation of the output power, and ultrasound detection is realized by recording the optical output power. High detector sensitivity requires high slope, which can be achieved by high resonance quality factor (Q). Polymer microring devices were fabricated on a 4-μm-thick SiO2 on a Si substrate using nanoimprinting technique [14]. With an improved technique in the mold fabrication and the design of operating wavelength around 780 nm [15] where the absorption loss of polymer and surrounding water cladding is minimized, an ultra-high Q factor of 3.0×10^5 was achieved. The microrings used in this study have a size of 60 μm in diameter and the polymer waveguides have a cross section of 1.0×1.4 μm^2 as shown in Fig. 1(b) and 1(c). A single-mode and a multi-mode optical fiber were aligned with the input and output of the straight waveguide, respectively, and then fixed using UV curable epoxy. Polymer microring device is favorable in POPAM because of its ultra-low noise and broad bandwidth [12, 15]. A much lower noise equivalent pressure (NEP) compared with other types of optical resonant structures [11] has been demonstrated and further improvement of NEP is possible by designing much higher-Q device and/or by coupling more power into waveguides. From the optical point of view, the detector's response time will be limited by the cavity's photon lifetime which is the time required for energy to decay to its original value

#142134 - $15.00 USD Received 9 Feb 2011; revised 4 Apr 2011; accepted 10 Apr 2011; published 25 Apr 2011

and is given by $\tau = Q/\omega$ [17]. Inverse of the response time will give the cut-off frequency. So our current device's frequency response can be up to 6.7GHz. From the acoustic point of view, a maximum modulation frequency of 570 MHz can be estimated considering the 1.4-μm-thick PS waveguide and the acoustic impedance of the cladding, polymer, and the substrate [16]. By designing the PS thickness less than 0.8 μm, microrings with a bandwidth limit of more than 1 GHz can be realized. If assuming strong acoustic reflections from the rigid substrate and negligible reflections from the cladding-polymer boundary, an approximated formula gives a quick estimation on the bandwidth limit:

$$|P_l(k)| = \frac{2|\sin(kl)|}{kl}, \tag{1}$$

where P is the mean distribution of stress across the thickness l of the sensing film due to an normally incident plane acoustic wave with wave number k. The POPAM with microrings has the potential to achieve higher axial resolution if more broadband signals can be detected, which requires a photodetector with higher frequency response than used in the current experiment.

The lateral resolution of the POPAM was measured by imaging an USAF resolution template (T-20-P-TM, Applied Image Inc, NY). Figure 1(d) shows the maximum amplitude projection (MAP) image of the resolution template, where the 6 bar elements of the group 7 can be resolved with the gaps up to 2.19 μm with modulation transfer function (MTF) value of 34%. Fitting the MTF to 50% yields a lateral resolution of 5 μm. The PAM with Onda transducer shows the same lateral resolution because they share the same optical focusing and scanning architecture which determines the lateral resolution of the system. In tissue imaging, the lateral resolution will deteriorate mildly due to the optical scattering. However, when the sample is optically thin (i.e. within one mean free path), the deterioration of the lateral resolution is insignificant [6, 7]. To quantify the axial resolution, typical A-line signals extracted from the images of the USAF resolution template were used as approximations of axial point-spread-functions (PSFs). Figure 1(e) depicts the axial PSF of POPAM; while Fig. 1f depicts the axial PSF of conventional PAM with Onda transducer. According to Rayleigh criterion, the PSFs show that this initial experiment of POPAM based on the microring resonator provided an axial resolution of 8 μm, close to the lateral optical resolution achieved; while PAM based on the Onda transducer gave a much larger axial resolution of 105 μm.

The bladder excised freshly from CD1 mouse (CD1, Charles River, MA) was imaged ex vivo. The MAPs (Fig. 2) of the images of the vasculature of the mouse bladder acquired with POPAM (upper row) and conventional PAM with Onda transducer (lower row) show the same views in the sample, since the POPAM and PAM shared the same optical scanning and the sample was not moved between scans. MAPS on the XY planes acquired with POPAM and PAM render a consistent structure of the bladder vasculature with same resolutions. The difference of the contrast distributions between them is due to the different positions of the microring resonator and onda transducer, one working in transmission mode and another working in reflection mode. MAPS on the XZ and YZ planes acquired with PAM indicated a tail-trail from microscale vessels along the axial direction, initially thought to be due to the limited bandwidth of the Onda transducer. The tail trail has a length over the depth of the sample and blurs the structures of the larger vessels. It is worth noting that the tail-trail effect in the PAM is not as apparent for the larger vessels, implying that the effect is also related to a different mechanism of light and/or sound transport around or through the vessels. MAPS on the XZ and YZ plane acquired with POPAM indicated no tail-trail effect. The microscale capillary net with apparently large vasculature hiding in it can be clearly rendered. All the images in Fig. 2 were acquired without averaging and proving maximum contrast to noise ratios of 26dB for POPAM and 29dB for PAM. The commercial Onda transducer has a high sensitivity providing noise equivalent detectable pressure (NEDP) value of 19Pa. The results of POPAM give an estimation of the sensitivity of the microring resonator of NEDP value of

#142134 - $15.00 USD Received 9 Feb 2011; revised 4 Apr 2011; accepted 10 Apr 2011; published 25 Apr 2011

29Pa, comparable to the Onda transducer, which is much higher than other optical resonant structures available for acoustic measurement with NEDP on the order of magnitude of hundreds of Pascal.

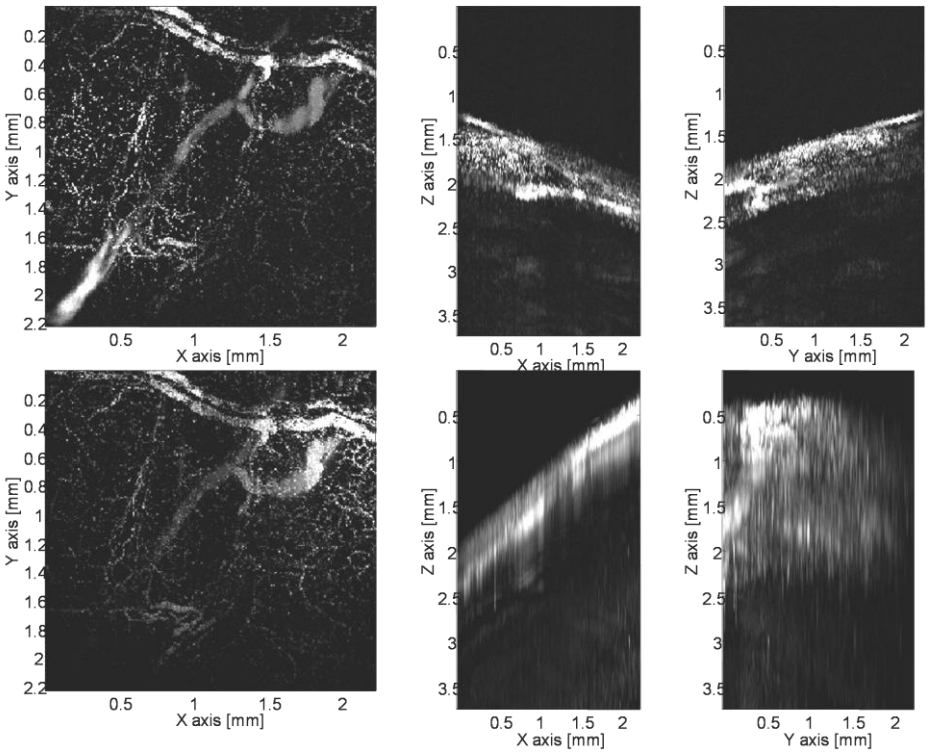

Fig. 2. MAPs on XY, XZ, YZ planes of the ex vivo images of the vasculature in a mouse bladder wall acquired with POPAM (upper row) using microring and conventional PAM using Onda transducer (lower row).

The high sensitivity of the microring resonator provides POPAM with the ability to detect the weak signal even from individual red blood cells. To verify this, we prepared a CD1 mouse bladder which was stored at 5°C for 48 hours after excision before imaging. Figure 3(a) shows its photo and Fig. 3(b) shows its MAP image on XY plane with POPAM, indicating that individual blood cells can be discerned clearly by POPAM with a curvilinear alignment along a capillary. Some larger dots with size of tens of um are agglomerations of several blood cells. We have also verified the feasibility of POPAM for in vivo imaging of vasculature through the experiment on the ear of CD1 mouse with body weight 30g. The animal experiment has been approved by the UCUCA of the University of Michigan. Before imaging, 0.03ml Ketaset with ketamine 100mg/ml was injected to anesthetize the mouse and hairs on the ear were removed using hair-removing lotion. The photo and MAP image of mouse ear are shown in Fig. 3(c) and 3(d) respectively. The branching of vessels at different deep layers can be clearly observed. Some smallest vessels have diameters of ~5μm and are on the capillary level. The interesting thing is that most of single capillaries imaged in the in vivo mouse ear present the continuous tubular structure different with the discrete distribution of individual red blood cells imaged in the ex vivo mouse bladder. It is probably due to the flowing of blood cells and high concentration of blood cells in the microvasculature in the case of in vivo imaging.

#142134 - $15.00 USD Received 9 Feb 2011; revised 4 Apr 2011; accepted 10 Apr 2011; published 25 Apr 2011

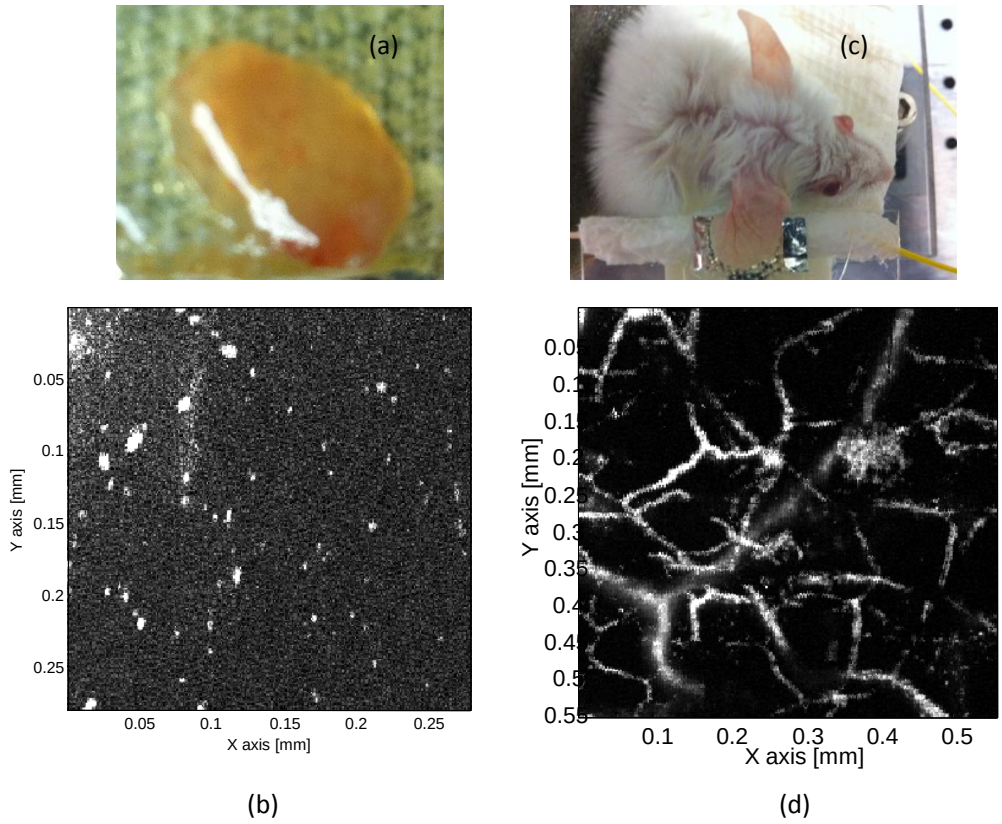

Fig. 3. Photos of mouse bladder *ex vivo* (a) and mouse ear *in vivo* (c). MAPs on XY planes from POPAM imaging mouse bladder *ex vivo* (b) and POPAM imaging mouse ear *in vivo* (d).

3. Discussion and conclusion

A new POPAM was validated for the first time in this paper for its unique axial resolution by using a small fraction of the superbroad bandwidth optical microring resonator. The microring resonator was designed with an extremely high Q value, providing high sensitivity with a NEDP value of 29Pa. The sensitivity could be improved by further reducing sidewall roughness of the microring to achieve much higher Q value and with higher laser input power. The 3D structure of capillary networks and other microvasculature and even individual red blood cells have been discerned successfully in the proof-of-concept experiments on mouse bladders and ears. The lateral resolution of 5 μm and axial resolution of 8 μm provided by the POPAM could be improved by increasing the numerical aperture of the objective lens from its value of 0.51. The achieved axial resolution was limited to well below the microring's theoretical potential. With the increased bandwidth of a more polished microring detector and wider bandwidth low noise photodiode detector, the axial resolution should be increased by a large amount, with corresponding drop in acoustic imaging depth in the sample.

POPAM can provide 3D resolution comparable to optical microscopy but quite different contrast information, with sensitivity to optical absorption and thermal coefficient of expansion, as well as optical fluence. Thus it is sensitive to the vasculature, and distribution of oxygen and water concentration. The miniaturized size of the microring detector and the biocompatibility of pure optical photoacoustic microscopy open an opportunity to noninvasive endoscopic imaging of a variety of diseases such as breathing disorders, chronic diarrhea, incontinence, internal bleeding, irritable bowel syndrome, stomach ulcers and urinary tract infections. The microring resonator has a diameter of 60 microns and is already fiber-connected, well suited for endoscopic imaging.

#142134 - $15.00 USD Received 9 Feb 2011; revised 4 Apr 2011; accepted 10 Apr 2011; published 25 Apr 2011

This work was initiated to consider sensitive, small elements for large arrays with scalable imaging ability from microscale to macroscale. The cost of construction of such arrays is a difficulty at this time, but they remain good possibilities for the future, with their extremely broad bandwidth and high sensitivity.

Acknowledgments

Support from NIH Grant No. R01 EB007619, R01 CA91713, CA91713-S1 and R01 AR055179 are gratefully acknowledged.

#142134 - $15.00 USD Received 9 Feb 2011; revised 4 Apr 2011; accepted 10 Apr 2011; published 25 Apr 2011